

# Infrared Properties of SiO Maser Sources in Late-Type Stars

Mikako MATSUURA,<sup>1,2</sup> Issei YAMAMURA,<sup>3,1</sup> Hiroshi MURAKAMI,<sup>1</sup> Takashi ONAKA,<sup>2</sup>  
Takafumi OOTSUBO,<sup>2</sup> Takanao TOHYA,<sup>1,2</sup> Yoshihiko OKAMURA,<sup>1,4</sup>  
Minoru M. FREUND,<sup>1,5</sup> and Masahiro TANAKA<sup>1</sup>

<sup>1</sup>*The Institute of Space and Astronautical Science (ISAS),  
3-1-1 Yoshinodai, Sagami-hara, Kanagawa 229-8510*

<sup>2</sup>*Department of Astronomy, The University of Tokyo,  
7-3-1 Hongo, Bunkyo, Tokyo 113-0033*

<sup>3</sup>*Astronomical Institute ‘Anton Pannekoek’, University of Amsterdam,  
Kruislaan 403, 1098 SJ, Amsterdam, The Netherlands*

<sup>4</sup>*Department of Physics, The University of Tokyo,  
7-3-1 Hongo, Bunkyo, Tokyo 113-0033*

<sup>5</sup>*Infrared Astrophysics Branch, Code 685,  
NASA Goddard Space Flight Center, Greenbelt, MD 20771, USA  
E-mail (MM): mikako@ir.isas.ac.jp*

(Received 2000 January 13; accepted 2000 May 31)

## Abstract

The results of an SiO maser survey for late-type stars selected by the IRTS (Infrared Telescope in Space) are presented. We have detected SiO  $J = 1-0$ ,  $v = 1$  and/or  $v = 2$  lines in 27 stars out of 59 stars. The maser intensity increases with the depth of the H<sub>2</sub>O absorption in the infrared spectra and redness of the 2.2 and 12  $\mu\text{m}$  color. The column densities of the water vapor in the target stars were estimated from the depth of the water absorption in the IRTS spectra. We found that the SiO maser was detected mostly in the stars with a column density of water vapor higher than  $3 \times 10^{19}$ – $3 \times 10^{20}$   $\text{cm}^{-2}$ . We further estimated the density of hydrogen molecules in the outer atmosphere corresponding to these column densities, obtaining  $10^9$ – $10^{10}$   $\text{cm}^{-3}$  as a lower limit. These values are roughly in agreement with the critical hydrogen density predicted by models for the excitation of SiO masers. It is possible that the SiO masers are excited in clumps with column density even higher than this value. The present results provide useful information for the understanding of the physical conditions of the outer atmospheres in late-type stars.

**Key words:** infrared: stars — radio lines: stars — stars: atmospheres — stars: late-type — stars: long period variables

## 1. Introduction

One of the characteristics of red-giant stars is the possession of the atmosphere more extended than that in hydrostatic equilibrium. Several kinds of molecules are formed in the extended atmosphere. Dust grains are also formed in the outermost region of the extended atmosphere and, consequently, the mass loss is accelerated by radiation pressure on the dust grains. The extended atmosphere is thought to be generated by large pulsations of the stars. Woitke et al. (1999) showed theoretically that pulsation affects the density structure of the molecules, especially poly-atomic molecules. However, poly-atomic molecules, such as H<sub>2</sub>O, CO<sub>2</sub>, and SO<sub>2</sub>, are difficult to observe from the ground because of interference by the terrestrial atmosphere. Recent observations based on satellite missions allowed investigations of the

properties of these molecules in the extended atmosphere (Tsuji et al. 1997; Justtanont et al. 1998; Ryde et al. 1999; Yamamura et al. 1999a, b). Tsuji et al. (1997) found that a layer of molecules, which the authors called a “warm molecular envelope”, is also present in non-Mira variables, i.e., irregular and semi-regular variables. The pulsations of these stars are rather weak, and it is under discussion at present whether the pulsation is still responsible for the formation of the molecular layer, even in non-Mira variables. Hereafter, we denote the extended atmosphere or the warm molecular envelope as an “outer atmosphere”, which is the region located above the photosphere, but below the circumstellar envelope (see also Yamamura, de Jong 2000).

Matsuura et al. (1999; hereafter Paper I) have studied the water-vapor absorption band at 1.9  $\mu\text{m}$  based on

Table 1. List of SiO  $J = 1-0$ ,  $v = 1$  and/or  $v = 2$  masers detected sources.

IRAS name	R.A. (B1950)	Dec. (B1950)	$I_{\text{H}_2\text{O}}$	$C_{2.2/1.7}$	GCVS name	Type	Comment
02255+6903	02 <sup>h</sup> 25 <sup>m</sup> 33 <sup>s</sup> .8	+69 <sup>d</sup> 03 <sup>m</sup> 36 <sup>s</sup> .0	0.074	0.015			
04081+5832	04 <sup>h</sup> 08 <sup>m</sup> 06 <sup>s</sup> .8	+58 <sup>d</sup> 32 <sup>m</sup> 22 <sup>s</sup> .0	0.171	0.015			
06266-1148	06 <sup>h</sup> 26 <sup>m</sup> 36 <sup>s</sup> .1	-11 <sup>d</sup> 48 <sup>m</sup> 58 <sup>s</sup> .0	0.286	0.084			
07019-1631	07 <sup>h</sup> 01 <sup>m</sup> 58 <sup>s</sup> .0	-16 <sup>d</sup> 31 <sup>m</sup> 02 <sup>s</sup> .0	0.328	0.007			
07232-0544	07 <sup>h</sup> 23 <sup>m</sup> 13 <sup>s</sup> .0	-05 <sup>d</sup> 44 <sup>m</sup> 59 <sup>s</sup> .0	0.234	-0.047	TT Mon	M	1)
07268-0410	07 <sup>h</sup> 26 <sup>m</sup> 52 <sup>s</sup> .0	-04 <sup>d</sup> 10 <sup>m</sup> 30 <sup>s</sup> .0	0.022	-0.035	RX Mon	M	
08186+1409	08 <sup>h</sup> 18 <sup>m</sup> 36 <sup>s</sup> .6	+14 <sup>d</sup> 09 <sup>m</sup> 49 <sup>s</sup> .0	0.172	-0.035	SZ Cnc	M	
12341+5945	12 <sup>h</sup> 34 <sup>m</sup> 07 <sup>s</sup> .0	+59 <sup>d</sup> 45 <sup>m</sup> 42 <sup>s</sup> .9	0.192	-0.060	T UMa	M	
18076+3445	18 <sup>h</sup> 07 <sup>m</sup> 37 <sup>s</sup> .0	+34 <sup>d</sup> 45 <sup>m</sup> 40 <sup>s</sup> .0	0.301	0.288			
18156+0655	18 <sup>h</sup> 15 <sup>m</sup> 40 <sup>s</sup> .8	+06 <sup>d</sup> 55 <sup>m</sup> 01 <sup>s</sup> .0	0.228	0.002	BC Oph	M	
18186+3143	18 <sup>h</sup> 18 <sup>m</sup> 37 <sup>s</sup> .6	+31 <sup>d</sup> 43 <sup>m</sup> 54 <sup>s</sup> .0	0.101	-0.055	TU Lyr	Lb	
18222+3933	18 <sup>h</sup> 22 <sup>m</sup> 18 <sup>s</sup> .0	+39 <sup>d</sup> 33 <sup>m</sup> 24 <sup>s</sup> .0	0.108	-0.027	TW Lyr	M	1)
18347+2600	18 <sup>h</sup> 34 <sup>m</sup> 45 <sup>s</sup> .0	+26 <sup>d</sup> 00 <sup>m</sup> 24 <sup>s</sup> .0	0.081	-0.039	RZ Her	M	
18394+2845 $\diamond$	18 <sup>h</sup> 39 <sup>m</sup> 29 <sup>s</sup> .9	+28 <sup>d</sup> 45 <sup>m</sup> 56 <sup>s</sup> .4	0.050	-0.070	SY Lyr	SRb	
18561+1642	18 <sup>h</sup> 56 <sup>m</sup> 10 <sup>s</sup> .0	+16 <sup>d</sup> 42 <sup>m</sup> 48 <sup>s</sup> .0	0.174	-0.028	EU Aql	M	2)
19090+1746	19 <sup>h</sup> 09 <sup>m</sup> 03 <sup>s</sup> .6	+17 <sup>d</sup> 46 <sup>m</sup> 48 <sup>s</sup> .0	0.108	0.024	KK Sge	M	2)
19158+1955	19 <sup>h</sup> 15 <sup>m</sup> 48 <sup>s</sup> .9	+19 <sup>d</sup> 55 <sup>m</sup> 54 <sup>s</sup> .0	0.103	-0.001	NO Sge	M	2)
19172+1706	19 <sup>h</sup> 17 <sup>m</sup> 18 <sup>s</sup> .0	+17 <sup>d</sup> 06 <sup>m</sup> 48 <sup>s</sup> .0	0.292	0.001	W Sge	M	2)
19285+4853	19 <sup>h</sup> 28 <sup>m</sup> 33 <sup>s</sup> .9	+48 <sup>d</sup> 53 <sup>m</sup> 45 <sup>s</sup> .0	0.101	-0.046			
19308+0609 $\diamond$	19 <sup>h</sup> 30 <sup>m</sup> 55 <sup>s</sup> .0	+06 <sup>d</sup> 09 <sup>m</sup> 30 <sup>s</sup> .0	0.059	-0.079	V 621 Aql	SRb	
19412+0337	19 <sup>h</sup> 41 <sup>m</sup> 15 <sup>s</sup> .3	+03 <sup>d</sup> 37 <sup>m</sup> 15 <sup>s</sup> .0	0.402	0.236	*		
19550-0201	19 <sup>h</sup> 55 <sup>m</sup> 01 <sup>s</sup> .0	-02 <sup>d</sup> 01 <sup>m</sup> 12 <sup>s</sup> .0	0.357	0.048	RR Aql	M	
20077-0625	20 <sup>h</sup> 07 <sup>m</sup> 46 <sup>s</sup> .0	-06 <sup>d</sup> 24 <sup>m</sup> 42 <sup>s</sup> .0	0.336	0.392	V 1300 Aql $\dagger$	M:	1)
20215+6243	20 <sup>h</sup> 21 <sup>m</sup> 32 <sup>s</sup> .3	+62 <sup>d</sup> 43 <sup>m</sup> 21 <sup>s</sup> .0	0.097	-0.004			
20234-1357	20 <sup>h</sup> 23 <sup>m</sup> 26 <sup>s</sup> .0	-13 <sup>d</sup> 57 <sup>m</sup> 51 <sup>s</sup> .0	0.236	0.061			
20296-2151	20 <sup>h</sup> 29 <sup>m</sup> 38 <sup>s</sup> .7	-21 <sup>d</sup> 51 <sup>m</sup> 40 <sup>s</sup> .0	0.332	0.016	RU Cap	M	
20305+6246	20 <sup>h</sup> 30 <sup>m</sup> 35 <sup>s</sup> .4	+62 <sup>d</sup> 46 <sup>m</sup> 28 <sup>s</sup> .0	0.078	0.014	BF Cep	M	

Note.  $\diamond$  indicates tentative detection. Type is variable type according to GCVS; M : Mira variable, SR : semi-regular variable, SRb : a sub-class of SR and indicate semi-regular variable with “poor defined periodicity”, Lb : irregular variable. Comments show the quality of NIRS spectra: 1) Confusion with other source(s) occurred, i.e., more than 2 sources entered in the field of view when the star was observed, because of the NIRS’s large aperture. Brightness of the fainter sources are about 20% of the target star at 2.2  $\mu\text{m}$ . 2) The flux quality is low, because of the different satellite operation near the galactic plane. About 10–20% flux uncertainty remains. \*IRC +00450.  $\dagger$ IRC -10529.

spectro-photometric data obtained by the Near-Infrared Spectrometer (NIRS; Noda et al. 1996) onboard the Infrared Telescope in Space (IRTS; Murakami et al. 1996). The NIRS observed water-vapor absorption in a large sample of stars. In the near-infrared region, the water vapor is a dominant absorber in red-giants. The water-vapor absorption bands are thought to arise mainly from the outer atmosphere of these stars. The strength of the water-vapor absorption increases with the 2.2 and 12  $\mu\text{m}$  color,  $C_{12/2.2}$ . This color is an indicator of the amount of dust in the inner part of the circumstellar shell. In Paper I, we suggested that the depth of the water-vapor absorption represents the amount of matter in the outer atmosphere, indicating a close relation between the density of the outer atmosphere and the mass-loss rate.

SiO masers have been detected in many oxygen-rich red-giants and red-supergiants. SiO molecules are con-

densed into dust in the region with a temperature of around 1000 K. SiO masers are thought to be excited in the region below the dust-forming region (Nyman, Olofsson 1986), i.e., in the outer atmosphere. VLBI observations detect SiO maser spots at 1–4 stellar radii from the central stars (Miyoshi et al. 1994; Diamond et al. 1994). The detection of these spots supports an idea proposed by Langer and Watson (1984) that the infalling wind makes inhomogeneous structures, and that strong SiO maser emission comes from high-density clumps. However, it is difficult to derive the properties of the outer atmosphere quantitatively only from the observations of the SiO masers, and to understand the circumstances for the excitation of SiO masers. Two pumping mechanisms have been proposed so far concerning the excitation of SiO masers: radiative pumping (e.g., Kwan, Scoville 1974; Deguchi, Iguchi 1976; Bujarrabal 1994a,

Table 2. List of SiO non-detected sources.

IRAS name	R.A. (B1950)	Dec. (B1950)	$I_{\text{H}_2\text{O}}$	$C_{2.2/1.7}$	GCVS name	Type	Comment
01010+7434	01 <sup>h</sup> 01 <sup>m</sup> 03 <sup>s</sup> .8	+74 <sup>d</sup> 34 <sup>m</sup> 00 <sup>s</sup> .1	0.013	-0.063			
01584+7103	01 <sup>h</sup> 58 <sup>m</sup> 26 <sup>s</sup> .8	+71 <sup>d</sup> 03 <sup>m</sup> 24 <sup>s</sup> .0	-0.005	-0.105			
03478+6349	03 <sup>h</sup> 47 <sup>m</sup> 53 <sup>s</sup> .3	+63 <sup>d</sup> 49 <sup>m</sup> 13 <sup>s</sup> .0	0.083	-0.035	BF Cam	M:	
04265+5718	04 <sup>h</sup> 26 <sup>m</sup> 31 <sup>s</sup> .9	+57 <sup>d</sup> 18 <sup>m</sup> 12 <sup>s</sup> .7	0.044	-0.073	RV Cam	SRb	
04554+4437	04 <sup>h</sup> 55 <sup>m</sup> 29 <sup>s</sup> .8	+44 <sup>d</sup> 37 <sup>m</sup> 07 <sup>s</sup> .0	0.063	-0.051			
05026+4447	05 <sup>h</sup> 02 <sup>m</sup> 38 <sup>s</sup> .5	+44 <sup>d</sup> 47 <sup>m</sup> 40 <sup>s</sup> .0	0.065	-0.037			
05176+3502	05 <sup>h</sup> 17 <sup>m</sup> 35 <sup>s</sup> .0	+35 <sup>d</sup> 02 <sup>m</sup> 24 <sup>s</sup> .0	0.073	-0.007	EE Aur	Lb	
06153-3100	06 <sup>h</sup> 15 <sup>m</sup> 23 <sup>s</sup> .9	-31 <sup>d</sup> 00 <sup>m</sup> 14 <sup>s</sup> .6	0.083	-0.063	EH CMa	M	
07186-1017	07 <sup>h</sup> 18 <sup>m</sup> 36 <sup>s</sup> .2	-10 <sup>d</sup> 17 <sup>m</sup> 03 <sup>s</sup> .0	0.128	-0.047	V 632 Mon	SR:	
07393-0403	07 <sup>h</sup> 39 <sup>m</sup> 18 <sup>s</sup> .5	-04 <sup>d</sup> 03 <sup>m</sup> 30 <sup>s</sup> .0	0.036	-0.056			
08196+1509	08 <sup>h</sup> 19 <sup>m</sup> 36 <sup>s</sup> .9	+15 <sup>d</sup> 09 <sup>m</sup> 11 <sup>s</sup> .1	0.041	-0.076	Z Cnc	SRb	
11538+5808	11 <sup>h</sup> 53 <sup>m</sup> 54 <sup>s</sup> .0	+58 <sup>d</sup> 09 <sup>m</sup> 00 <sup>s</sup> .0	0.058	-0.065	Z UMa	SRb	
16418+5459	16 <sup>h</sup> 41 <sup>m</sup> 52 <sup>s</sup> .0	+54 <sup>d</sup> 59 <sup>m</sup> 48 <sup>s</sup> .0	0.051	-0.055	S Dra	SRb	
16473+5753	16 <sup>h</sup> 47 <sup>m</sup> 24 <sup>s</sup> .0	+57 <sup>d</sup> 54 <sup>m</sup> 00 <sup>s</sup> .0	0.091	-0.085	AH Dra	SRb	
17359+4555	17 <sup>h</sup> 35 <sup>m</sup> 56 <sup>s</sup> .3	+45 <sup>d</sup> 55 <sup>m</sup> 58 <sup>s</sup> .0	0.044	-0.072			
17473+4542	17 <sup>h</sup> 47 <sup>m</sup> 22 <sup>s</sup> .0	+45 <sup>d</sup> 42 <sup>m</sup> 54 <sup>s</sup> .0	0.013	-0.081	V 337 Her	SRb	
18052+4326	18 <sup>h</sup> 05 <sup>m</sup> 17 <sup>s</sup> .1	+43 <sup>d</sup> 26 <sup>m</sup> 40 <sup>s</sup> .4	0.001	-0.093			
18064+4212	18 <sup>h</sup> 06 <sup>m</sup> 26 <sup>s</sup> .0	+42 <sup>d</sup> 12 <sup>m</sup> 54 <sup>s</sup> .0	0.041	-0.067	V 529 Her	SR	
18291+3836	18 <sup>h</sup> 29 <sup>m</sup> 11 <sup>s</sup> .0	+38 <sup>d</sup> 36 <sup>m</sup> 12 <sup>s</sup> .0	0.017	-0.115	KP Lyr	SR	
18401+2854	18 <sup>h</sup> 40 <sup>m</sup> 07 <sup>s</sup> .0	+28 <sup>d</sup> 54 <sup>m</sup> 30 <sup>s</sup> .0	0.076	-0.044	FI Lyr	SRb	
18505+3327	18 <sup>h</sup> 50 <sup>m</sup> 30 <sup>s</sup> .6	+33 <sup>d</sup> 27 <sup>m</sup> 29 <sup>s</sup> .0	0.042	-0.063	HM Lyr	Lb	
18512+3034	18 <sup>h</sup> 51 <sup>m</sup> 12 <sup>s</sup> .8	+30 <sup>d</sup> 34 <sup>m</sup> 08 <sup>s</sup> .0	0.085	-0.043			
19040+2416	19 <sup>h</sup> 04 <sup>m</sup> 03 <sup>s</sup> .3	+24 <sup>d</sup> 16 <sup>m</sup> 32 <sup>s</sup> .0	0.015	-0.093			
19194+1734	19 <sup>h</sup> 19 <sup>m</sup> 28 <sup>s</sup> .2	+17 <sup>d</sup> 34 <sup>m</sup> 14 <sup>s</sup> .0	0.048	-0.045	T Sge	SRb	2)
19267+0345	19 <sup>h</sup> 26 <sup>m</sup> 43 <sup>s</sup> .0	+03 <sup>d</sup> 45 <sup>m</sup> 30 <sup>s</sup> .0	0.051	-0.046	V 858Aql	Lb	
19306+0455	19 <sup>h</sup> 30 <sup>m</sup> 39 <sup>s</sup> .0	+04 <sup>d</sup> 55 <sup>m</sup> 12 <sup>s</sup> .0	-0.012	-0.097	V 1293 Aql	SRb	
19461+0334	19 <sup>h</sup> 46 <sup>m</sup> 07 <sup>s</sup> .0	+03 <sup>d</sup> 34 <sup>m</sup> 18 <sup>s</sup> .0	0.022	-0.090	WX Aql	SRb	
20073-1041	20 <sup>h</sup> 07 <sup>m</sup> 22 <sup>s</sup> .5	-10 <sup>d</sup> 41 <sup>m</sup> 04 <sup>s</sup> .6	0.046	-0.094	†		
20094-1121	20 <sup>h</sup> 09 <sup>m</sup> 29 <sup>s</sup> .3	-11 <sup>d</sup> 21 <sup>m</sup> 21 <sup>s</sup> .1	0.079	-0.050			
20161-1600	20 <sup>h</sup> 16 <sup>m</sup> 08 <sup>s</sup> .0	-16 <sup>d</sup> 00 <sup>m</sup> 54 <sup>s</sup> .0	0.085	-0.083	AE Cap	SR	
20311-2325	20 <sup>h</sup> 31 <sup>m</sup> 11 <sup>s</sup> .0	-23 <sup>d</sup> 25 <sup>m</sup> 18 <sup>s</sup> .0	0.024	-0.130	AK Cap	Lb	
22073+7231	22 <sup>h</sup> 07 <sup>m</sup> 23 <sup>s</sup> .0	+72 <sup>d</sup> 31 <sup>m</sup> 24 <sup>s</sup> .0	-0.008	-0.081	DM Cep	Lb	

Note. †SAO 163310. Comment 2) means the same as table 1.

b) and collisional pumping (e.g., Elitzur 1980; Doel et al. 1995). At present, it is not yet settled which mechanism is dominant in late-type stars.

The near- and mid-infrared observations by the IRTS provide useful information about the outer atmosphere. It is worth comparing the SiO maser properties with the parameters derived from near- and mid-infrared observations by the IRTS. Previous SiO maser surveys (e.g., Allen et al. 1989; Izumiura et al. 1994) were mostly based on the IRAS Point Source Catalog (IRAS-PSC; Joint IRAS Working Group 1988). The SiO detected sources and non-detected sources are uniformly scattered in the regions of oxygen-rich stars, and are not clearly separated on the IRAS color-color diagram (Haikala 1990). The SiO maser is much more frequently detected in Mira variables than in other variable types. Only a few semi-regular and irregular variables exhibit SiO maser activ-

ity. The non-Mira SiO maser sources usually have a visual amplitude larger than 2.5 mag (Alcolea et al. 1990), which is comparable to that of Mira variables. It is thus suggested that SiO maser excitation is related to stellar pulsation because stars with a larger visual amplitude are expected to have stronger pulsation. Alcolea et al. (1990) suggested that fewer detections of the SiO maser in semi-regular variables indicates a less-developed outer atmosphere in these stars, because the pulsation of semi-regulars is weaker than that of Miras.

In this paper, we report on the results of an SiO maser survey in a sample of the IRTS point sources. The IRTS provided a large number of stellar spectra in near- and mid-infrared regions, unaffected by the terrestrial atmosphere. The infrared colors and the strength of the water absorption are compared with the SiO maser intensity. We will discuss the conditions for exciting SiO masers.

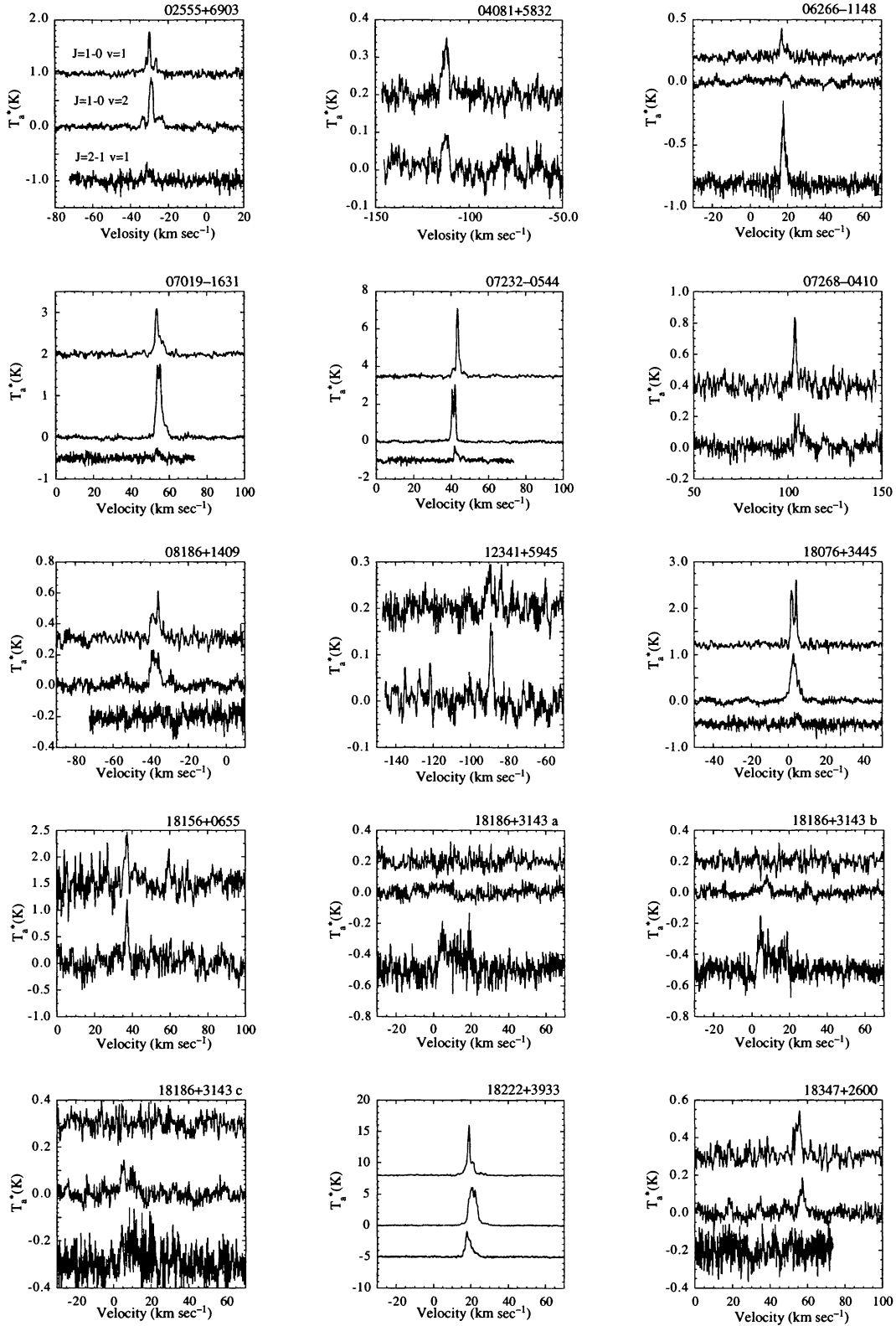


Fig. 1a. SiO maser spectra of detected sources are shown. From top to bottom, the spectra indicate  $J = 1-0$ ,  $v = 1$ ;  $J = 1-0$ ,  $v = 2$ ; and  $J = 2-1$ ,  $v = 1$  lines. When  $J = 2-1$ ,  $v = 1$  line was not observed, only two  $J = 1-0$  spectra are presented. IRAS 18186+3143 was observed three times, and all spectra are plotted.

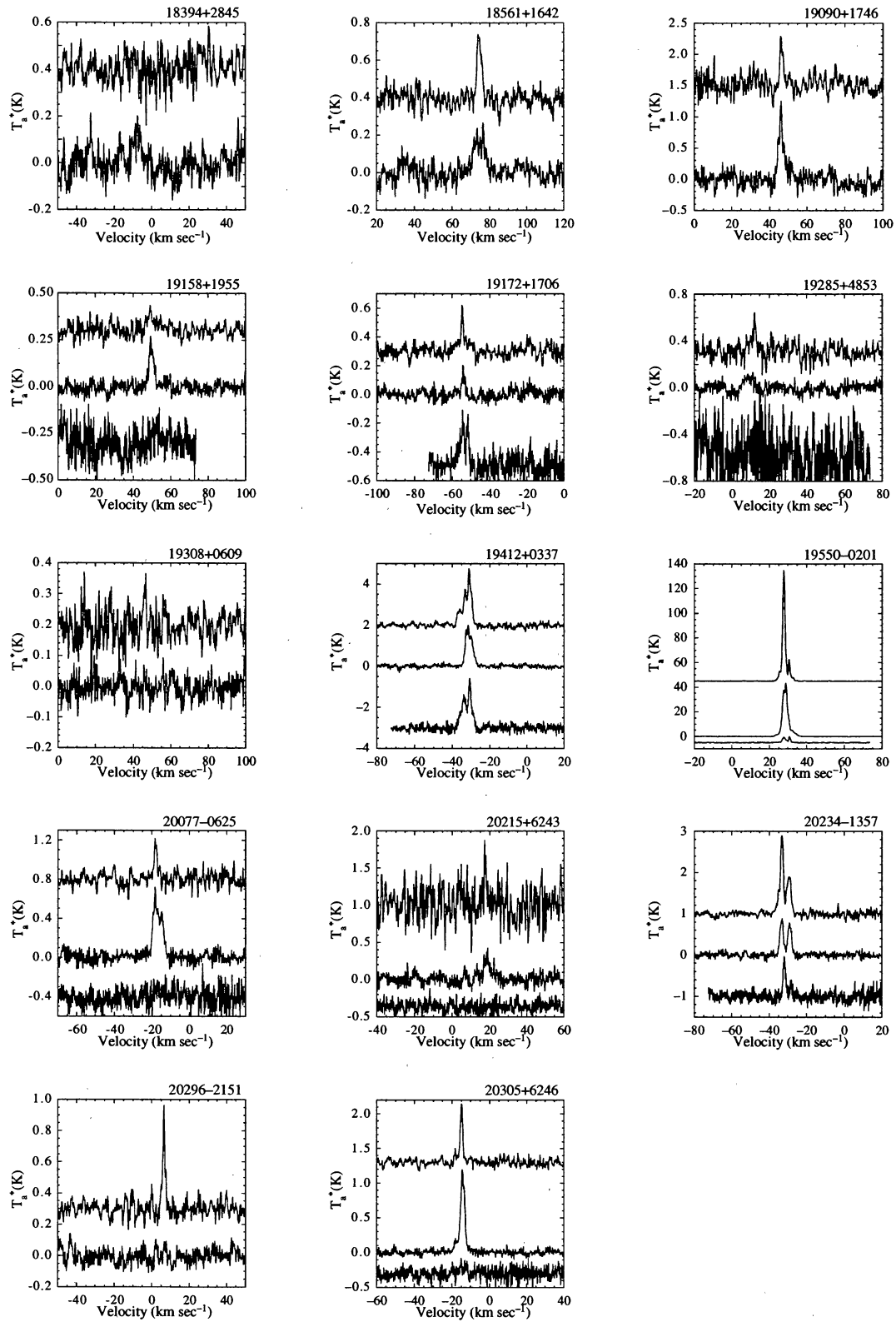


Fig. 1b. Same as figure 1a.

## 2. Observations

We conducted observations of SiO masers with the 45-m telescope at Nobeyama Radio Observatory in 1998 from May 20 to 25, and from June 10 to 12. We simultaneously observed three SiO maser lines:  $J = 1-0$ ,  $v = 1$  (43.1220 GHz),  $J = 1-0$ ,  $v = 2$  (42.8205 GHz), and  $J = 2-1$ ,  $v = 1$  (86.2434 GHz). Two cooled SIS receivers (S40 for 43 GHz, and S100 for 86 GHz) were used with acousto-optical spectrometers (AOS's). Each AOS covers 40 MHz with a resolution of 37 kHz. The velocity coverage is about  $\pm 140$  km s $^{-1}$  for the  $J = 1-0$  lines, and about  $\pm 70$  km s $^{-1}$  for the  $J = 2-1$  line, respectively. The overall system temperature at 43 GHz was typically 150–250 K with the worst case of 900 K, depending on the weather and the telescope elevation. The  $J = 2-1$  line was observed only when the conditions were appropriate, and the overall system temperature ranged between 300 and 450 K. The half-power beam width of the telescope is 40" at 43 GHz and 18" at 86 GHz, respectively. The conversion factors from antenna temperature ( $T_a^*$  in K) to flux density (Jy) are 2.0 Jy K $^{-1}$  at 43 GHz, and 2.6 Jy K $^{-1}$  at 86 GHz.

The target stars were selected from a preliminary list of the IRTS point sources, whose spectra were obtained by both the Mid-Infrared Spectrometer (MIRS; Roellig et al. 1996), and the NIRS. The selection criteria are: (1) The flux is approximately larger than 10 Jy at 10  $\mu$ m and larger than 1 Jy at 2.2  $\mu$ m. To obtain a wide coverage of different infrared colors and water indices, we also include some stars with flux below 10 Jy at 10  $\mu$ m. (2) The spectrum shows the characteristics of an oxygen-rich star (cf. Yamamura et al. 1997). Carbon-rich stars and S-type stars in the catalogues (Stephenson 1984, 1989) are excluded. (3) The star has an identification in the IRAS-PSC. In the present study, we include some stars near the galactic plane, which were not included in Paper I. The positions of the stars were taken from the IRAS-PSC, the General Catalogues of Variable Stars (GCVS; Kholopov et al. 1988), the Smithsonian Astrophysical Observatory Star Catalog (SAO; Smithsonian Institution 1966), and in a few cases from other catalogues.

## 3. Results

The SiO  $J = 1-0$ ,  $v = 1$  and/or  $v = 2$  maser lines were detected in 27 stars out of 59 target stars. The infrared properties of detected sources and non-detected sources are listed in tables 1 and 2. The results of SiO observations are presented in tables 3 and 4. The spectra of the SiO masers are shown in figure 1. The infrared colors  $C_{2.2/1.7}$  and  $C_{12/2.2}$ , and the water index  $I_{\text{H}_2\text{O}}$  in tables 1 and 2 are defined by

$$C_{2.2/1.7} = \log(F_{2.2}/F_{1.7}), \quad (1)$$

$$C_{12/2.2} = \log(F_{12}/F_{2.2}), \quad (2)$$

and

$$I_{\text{H}_2\text{O}} = \log(F_{\text{cont}}/F_{1.9}), \quad (3)$$

where  $F_{2.2}$ ,  $F_{1.7}$ ,  $F_{1.9}$  are the IRTS/NIRS flux densities in units of Jy at the 2.2, 1.7 and 1.9  $\mu$ m channels, respectively.  $F_{\text{cont}}$  is the continuum flux level at 1.9  $\mu$ m, which was calculated by linear interpolation between  $F_{1.7}$  and  $F_{2.2}$ .  $F_{12}$  is the IRAS 12  $\mu$ m flux.  $C_{2.2/1.7}$  is an indicator of spectral types for stars earlier than M6 (see Paper I). In the following discussion, we use the peak intensity of  $J = 1-0$ ,  $v = 2$  to represent the strength of the SiO masers of each star. The integrated intensity has almost a linear relation with the peak intensity. The relation between the peak intensities of  $J = 1-0$ ,  $v = 2$  and  $J = 1-0$ ,  $v = 1$  lines is also mostly linear.

One irregular variable, TU Lyr (= IRAS 18186+3143), shows a strong  $J = 2-1$ ,  $v = 1$  maser intensity, while the  $J = 1-0$ ,  $v = 1$  and  $v = 2$  lines are rather weak. This object has an unusually broad line-width of about 20 km s $^{-1}$  compared to line-widths of less than 10 km s $^{-1}$  for other stars.

## 4. Detection Rate of the SiO Masers and the Infrared Properties

### 4.1. IRAS Color-Color Diagram

The distribution of our sample on the IRAS color-color diagram is shown in figure 2. All of the sampled stars have a good IRAS flux quality at 12 and 25  $\mu$ m. Four stars with low quality at the 60  $\mu$ m band are not plotted in figure 2. The division on the color-color diagram is taken from van der Veen and Habing (1988). The sampled stars are mostly distributed in regions II and IIIa, which are for oxygen-rich AGB stars with a low mass-loss rate of the order of  $10^{-7} M_{\odot}$  yr $^{-1}$  (van der Veen, Habing 1988). Several stars are located in region VII, which is for carbon stars. However, the near-infrared spectra confirm their oxygen-rich nature. "Detection" in figure 2 indicates that either  $J = 1-0$ ,  $v = 1$  or  $J = 1-0$ ,  $v = 2$  lines are detected in that star. No clear distinction is seen between the detected sources and the non-detected sources on the IRAS color-color diagram. This result is consistent with previous studies (e.g., Haikala 1990).

### 4.2. Near-Infrared Color and Water Index

One of the purposes of this survey was to search for SiO masers in early M type stars with water absorption reported in Paper I. These stars are supposed to have developed an extended atmosphere already among the early M type stars observed by the NIRS and, thus, SiO masers might be excited. We observed two stars in this category visible from Nobeyama: AK Cap (M2) and

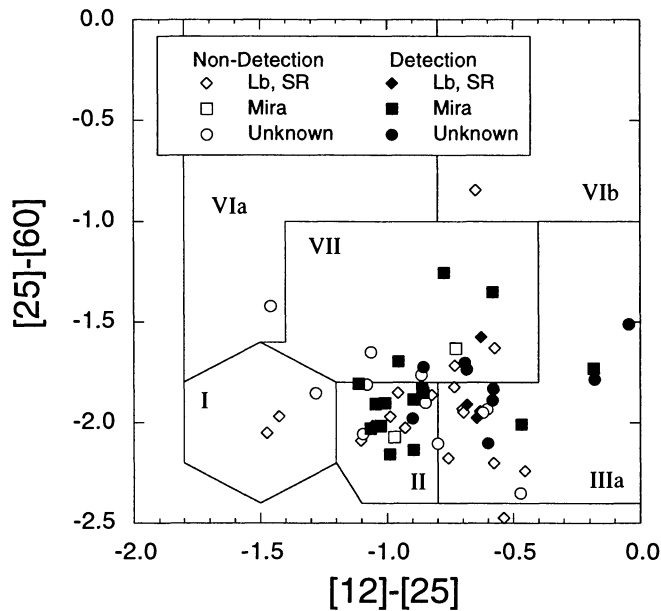


Fig. 2. Observed stars of our SiO maser survey plotted on the IRAS color-color diagram. The division of the regions comes from van der Veen and Habing (1988). The SiO detected stars are not well separated from the non-detected stars.

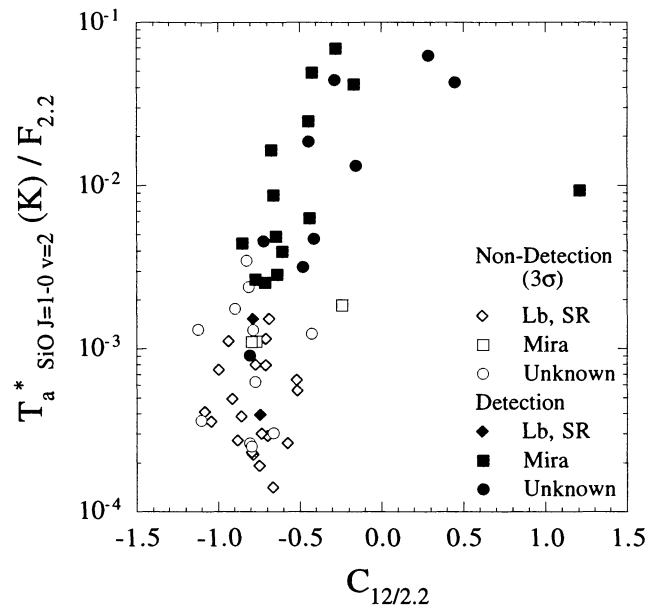


Fig. 4. SiO  $J = 1-0$ ,  $v = 2$  maser intensity plotted against  $C_{12/2.2}$ . For the non-detected stars,  $3\sigma$  ( $1\sigma$  is the rms level) is used for the maser intensity in this figure, which indicates the upper limit. To make the parameter independent of the distance, the SiO maser intensity is divided by  $F_{2.2}$ .  $C_{12/2.2}$  is an indicator of the mass-loss rate. There is a correlation between these indices in low mass-loss rate stars ( $C_{12/2.2} < 0.5$ , approximate dust mass-loss rate of  $7 \times 10^{-9} M_{\odot} \text{ yr}^{-1}$ ).

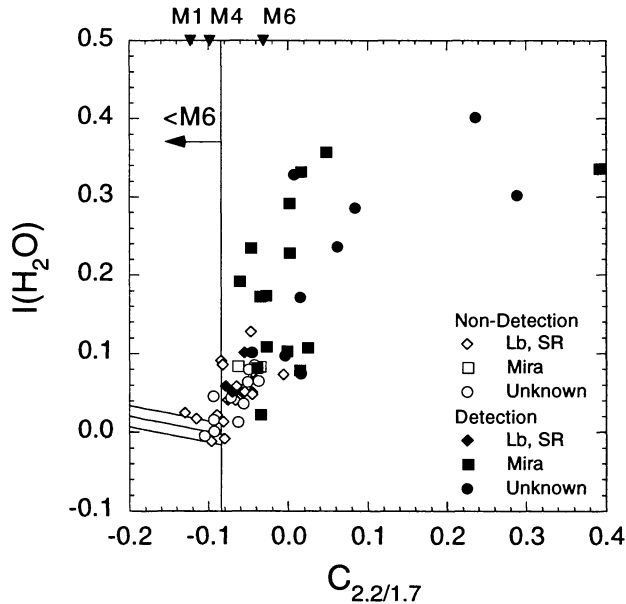


Fig. 3. Water index,  $I_{\text{H}_2\text{O}}$ , plotted as a function of  $C_{2.2/1.7}$ . The lines are from Paper I (see text). The symbols indicate SiO  $J = 1-0$  lines detection/non-detection, and variable types. The triangles on the upper side indicate the average color at each spectral type, derived from the sample in Paper I.

IRAS 20073–1041 (=SAO 163310, M3). However, SiO masers were not detected in either stars.

Figure 3 shows the distribution of the observed sources on the  $I_{\text{H}_2\text{O}}$  and  $C_{2.2/1.7}$  diagram. For reference, we plot several lines taken from figure 3 of Paper I. The three lines at the left bottom corner indicate the estimated zero level of the  $I_{\text{H}_2\text{O}}$  and  $C_{2.2/1.7}$  relation for stars without  $\text{H}_2\text{O}$  absorption, and the  $\pm 2\sigma$  deviations from that level. Stars above the  $+2\sigma$  line clearly exhibit water absorption (see figure 4 in Paper I).  $C_{2.2/1.7}$  is an indicator of spectral types for stars earlier than M6. Stars bluer than  $C_{2.2/1.7} < -0.085$  (vertical line) are expected to have spectral types earlier than M6. One M6 star, IRAS 19461+0334 (WX Aql), which was not included in Paper I, is actually located leftward of this vertical line; this will not affect our conclusions in this paper. In figure 3, a clear separation is seen between the SiO detected sources and the SiO non-detected sources. SiO masers are detected in stars with strong  $\text{H}_2\text{O}$  absorption ( $I_{\text{H}_2\text{O}}$  is approximately larger than 0.1). In addition, stars in the region of  $I_{\text{H}_2\text{O}}$  larger than  $\sim 0.1$  are mostly Mira variables when their variable types are known. SiO masers are seldom detected in non-Mira variables (see Habing 1996).

Table 3. Results of SiO maser observations for detected sources.

IRAS name	Date	$J = 1-0, v = 1$				$J = 1-0, v = 2$				$J = 2-1, v = 1$			
		rms	$V_{\text{LSR}}$	$T_{\text{a}}^*$	$S_{\text{a}}^*$	rms	$V_{\text{LSR}}$	$T_{\text{a}}^*$	$S_{\text{a}}^*$	rms	$V_{\text{LSR}}$	$T_{\text{a}}^*$	$S_{\text{a}}^*$
02255+6903	5.20	0.04	-29.7	0.78	2.19	0.04	-28.9	0.92	3.16	0.07	-31.1	0.35	0.64
04081+5832	5.20	0.02	-111.9	0.15	0.47	0.02	-112.9	0.10	0.34	.	.	.	.
06266-1148	6.11	0.02	16.9	0.23	0.55	0.02	18.6	0.09	0.19	0.05	17.7	0.65	1.16
07019-1631	6.12	0.04	53.7	1.10	3.24	0.03	55.4	1.76	6.33	0.06	54.0	0.25	0.41
07232-0544	5.20	0.04	43.5	3.59	6.29	0.04	42.1	3.05	6.13	0.07	41.7	0.79	1.58
07268-0410	5.20	0.04	103.6	0.43	0.74	0.04	105.6	0.22	0.75	.	.	.	.
08186+1409	6.11	0.03	-36.0	0.31	0.10	0.03	-38.3	0.23	0.90	0.04	.	.	.
12341+5945	5.21	0.02	-83.3	0.10	0.38	0.02	-89.0	0.17	0.33	.	.	.	.
18076+3445	5.23	0.04	4.1	1.40	3.67	0.04	2.7	1.03	4.41	0.06	3.2	0.26	0.65
18156+0655	6.10	0.16	37.4	0.97	1.85	0.15	37.3	1.20	2.00	.	.	.	.
18186+3143(a)	5.22	0.03	.	.	.	0.03	.	.	.	0.05	19.1	0.37	1.97
18186+3143(b)	5.23	0.03	.	.	.	0.03	8.0	0.11	0.32	0.04	4.7	0.35	1.76
18186+3143(c)	6.11	0.03	.	.	.	0.03	5.6	0.14	0.61	0.05	8.4	0.24	.
18222+3933	5.23	0.04	18.9	7.95	20.04	0.04	20.6	6.07	31.42	0.06	17.9	4.04	14.15
18347+2600	5.24	0.03	55.7	0.24	0.85	0.03	57.3	0.19	0.58	0.05	.	.	.
18394+2845	5.24	0.04	.	.	.	0.04	-7.5	0.20	0.65	.	.	.	.
18561+1642	5.25	0.04	73.9	0.34	0.94	0.04	76.4	0.27	1.22	.	.	.	.
19090+1746	6.10	0.10	46.0	0.79	1.40	0.10	46.2	1.25	3.66	.	.	.	.
19158+1955	6.11	0.03	49.0	0.14	0.61	0.03	49.4	0.27	0.75	0.06	.	.	.
19172+1706	5.23	0.04	-54.7	0.32	0.91	0.03	-54.2	0.20	0.38	0.06	-54.5	0.39	1.40
19285+4853	5.24	0.05	12.0	0.34	0.88	0.04	11.2	0.13	0.39	0.17	.	.	.
19308+0609	5.24	0.04	46.6	0.17	0.17	0.03	.	.	.	0.14	.	.	.
19412+0337	5.23	0.08	-31.1	2.76	11.06	0.07	-31.5	2.01	8.01	0.12	-30.8	2.42	9.97
19550-0201	5.23	0.09	27.7	89.96	180.57	0.08	28.8	43.45	153.45	0.13	30.7	4.99	16.29
20077-0625	5.23	0.05	-18.2	0.42	0.93	0.05	-18.2	0.72	3.34	0.07	.	.	.
20215+6243	5.20	0.18	17.2	0.88	0.81	0.07	18.9	0.42	1.66	0.04	.	.	.
20234-1357	6.11	0.05	-33.3	1.90	6.78	0.05	-33.1	0.88	3.89	0.10	-32.1	0.98	1.90
20296-2151	6.10	0.04	6.4	0.66	0.73	0.03	.	.	.	.	.	.	.
20305+6246	6.11	0.04	-14.9	0.85	1.66	0.03	-14.5	1.19	3.55	0.07	-15.1	0.22	0.37

Note. Date is observed day on 1998 M.DD. Rms is root-mean-square of the antenna temperature (K),  $V_{\text{LSR}}$  is velocity at intensity peak ( $\text{km s}^{-1}$ ),  $T_{\text{a}}^*$  is antenna temperature at peak (K),  $S_{\text{a}}^*$  is integrated intensity ( $\text{K km s}^{-1}$ ).

The present study confirms the same trend. The numbers of the SiO maser detected sources and non-detected sources for different variable types are summarized in table 5. SiO masers are detected with a high probability in Mira variables, while they are hardly detected in semi-regular variables and irregular variables.

## 5. Relation between the SiO Maser Intensity and the Infrared Parameters

### 5.1. Near- and Mid-Infrared Color

The infrared color  $K - [12]$  is considered to be an indicator of the mass-loss rate for Mira variables (Whitelock et al. 1994; Le Sidaner, Le Bertre 1996). We use  $C_{12/2.2}$  instead of  $K - [12]$ , because the  $F_{2.2}$  band represents the continuum level in  $K$ . The relation between the SiO maser intensity and the  $C_{12/2.2}$  is shown in figure 4. We plot the SiO maser intensity divided by  $F_{2.2}$ . We implicitly

assume that the intrinsic  $2.2 \mu\text{m}$  band luminosities of the sample stars are similar, and that the extinction by circumstellar dust is small in the  $2.2 \mu\text{m}$  band, except for a few extremely red stars. In figure 4, the SiO maser intensity seems to correlate with  $C_{12/2.2}$  in the color range  $C_{12/2.2} < 0.5$ . The SiO maser intensity increases with the mass-loss rate. The color  $C_{12/2.2} = +0.5$  corresponds to a dust mass-loss rate of approximately  $7 \times 10^{-9} M_{\odot} \text{ yr}^{-1}$ . Here, we use the equations in Le Sidaner and Le Bertre (1993, 1996); the zero magnitude flux of  $F_{2.2}$  is equal to 625 Jy (Cohen 1997). We assume the inner radius of the dust shell to be  $2.5 \times 10^{14} \text{ cm}$  and the expanding velocity to be  $10 \text{ km s}^{-1}$ .

Nyman and Olofsson (1986) suggested that the SiO maser intensity does not correlate with the mass-loss rate. They use a mass-loss rate calculated from the CO  $J = 1-0$  thermal emission. The CO emission is usually dominated by the molecules in the outer region of the



Table 4. Root mean square (rms) noise level of SiO maser observations for non-detected sources.\*

IRAS name	Date	$J = 1-0$	$J = 1-0$	$J = 2-1$
		$v = 1$ rms	$v = 2$ rms	$v = 1$ rms
01010+7434.....	5.20	0.03	0.03	0.05
01584+7103.....	6.11	0.03	0.03	0.07
03478+6349.....	6.11	0.03	0.03	0.05
04265+5718.....	5.20	0.03	0.03	0.04
04265+5718.....	6.12	0.03	0.03	0.05
04554+4437.....	6.12	0.03	0.03	0.04
05026+4447.....	5.20	0.03	0.03	0.05
05026+4447.....	6.12	0.02	0.02	0.04
05176+3502.....	5.20	0.04	0.04	0.08
06153-3100.....	6.12	0.04	0.04	0.07
07186-1017.....	6.12	0.03	0.03	0.04
07186-1017.....	6.11	0.03	0.03	0.05
07393-0403.....	5.20	0.03	0.03	0.06
08196+1509.....	6.12	0.02	0.02	0.04
08196+1509.....	5.21	0.03	0.03	0.05
11538+5808.....	5.21	0.03	0.03	0.05
16418+5459.....	5.23	0.03	0.03	0.05
16473+5753.....	5.23	0.03	0.03	0.05
17359+4555.....	5.24	0.05	0.05	.
17473+4542.....	5.23	0.03	0.03	0.05
18052+4326.....	5.22	0.03	0.03	0.05
18064+4212.....	5.23	0.04	0.04	0.07
18064+4212.....	5.22	0.04	0.04	0.07
18291+3836.....	5.23	0.03	0.03	0.06
18291+3836.....	6.11	0.06	0.07	.
18401+2854.....	6.11	0.04	0.04	0.08
18401+2854.....	5.23	0.03	0.03	0.07
18505+3327.....	6.11	0.04	0.04	0.09
18512+3034.....	5.25	0.07	0.07	.
19040+2416.....	5.23	0.04	0.03	0.06
19194+1734.....	6.10	0.05	0.05	.
19267+0345.....	5.24	0.03	0.03	0.06
19267+0345.....	6.10	0.03	0.03	.
19306+0455.....	5.24	0.03	0.03	0.06
19461+0334.....	5.24	0.03	0.03	0.09
19461+0334.....	5.23	0.04	0.04	0.06
20073-1041.....	5.23	0.04	0.03	0.06
20094-1121.....	5.24	0.03	0.03	0.07
20161-1600.....	5.24	0.03	0.03	0.06
20161-1600.....	6.11	0.03	0.03	0.06
20311-2325.....	5.23	0.03	0.02	0.05
22073+7231.....	5.20	0.03	0.03	0.05
22073+7231.....	6.11	0.03	0.03	0.08

\*Rms is in the unit of K.

circumstellar envelope. Therefore, it represents a mass-loss rate averaged over the past thousands years. On the other hand, since  $K - [12]$  or  $C_{12/2.2}$  represents emission from hot dust in the inner envelope, these colors indicate the recent mass-loss rate of the star. Since SiO masers are thought to be excited just below the dust forming

region, it is likely that the SiO maser intensity correlates better with  $C_{12/2.2}$  than the CO emission.

Table 5. The distribution of detected and non-detected sources at each variable type.

Type	Detected	Non-detected
Mira .....	15	2
SR .....	2	14
Lb .....	1	5
Unknown .....	9	11
Total	27	32

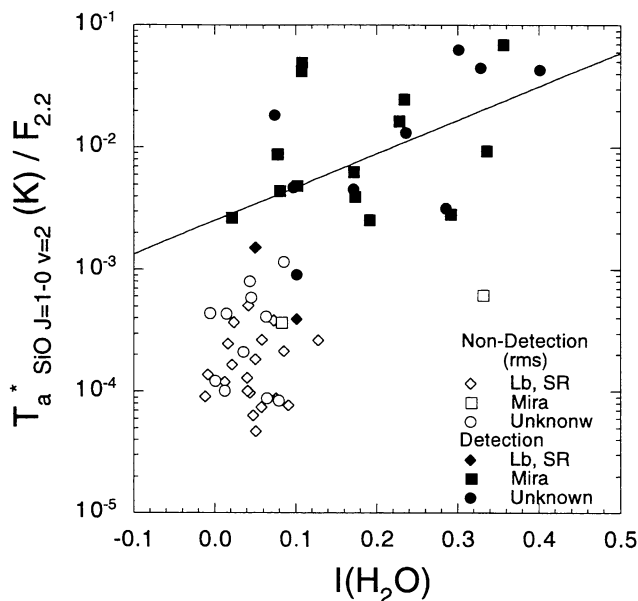


Fig. 5. Relation between the water index,  $I_{\text{H}_2\text{O}}$ , and the SiO maser intensity. For non-detected sources, we indicate  $3\sigma$  level for  $T_a^*$  as an upper limit. Only a weak relation is seen between  $I_{\text{H}_2\text{O}}$  and the SiO maser intensities.

### 5.2. Water Index

The SiO maser intensity is shown as a function of  $I_{\text{H}_2\text{O}}$  in figure 5. In general, the SiO maser intensity among the detected stars increases with  $I_{\text{H}_2\text{O}}$ , but the scatter is large. The large scatter might come from the time variation of the water absorption and the SiO maser intensity. In Mira variables, the water absorption depth changes from phase to phase (Hyland 1974), and the column density of water changes by a factor of 10 (Hinkle, Barnes 1979). The SiO maser intensity also varies by up to a factor of 10 (Nyman, Olofsson 1986; Alcolea et al. 1999). The variabilities in both quantities might obscure the relation between the water index and the SiO maser intensity.

## 6. Discussion

Figures 3 and 5 indicate that the sources showing the SiO maser lines have an  $I_{\text{H}_2\text{O}}$  larger than  $\sim 0.1$ , and that they are mostly Mira variables. Since the water index,  $I_{\text{H}_2\text{O}}$ , roughly indicates the column density of water molecules in the outer atmosphere, it is suggested that water column density is systematically different between the SiO maser detected stars and non-detected stars, and also between Miras and non-Miras. SiO masers are known to be detected quite often in Mira variables, while they are hardly detected in non-Miras (see Habing 1996). Alcolea et al. (1990) interpreted this in terms of the idea that the outer atmosphere is more “developed” in Miras than in non-Miras. Miras have stronger pulsation than non-Miras. Stronger pulsation would lift up more matter from the photosphere into the outer atmosphere, leading to a higher density and thus higher column density of the molecules. Our results about the relation with  $I_{\text{H}_2\text{O}}$  indicate that the high detection rate of the SiO maser in Miras is related to the high column density in the outer atmosphere.

The column densities of water molecules have been measured for several stars. In table 6, we summarize the results of near-infrared observations of the  $\text{H}_2\text{O}$  bands reported in Paper I and other literature. In Paper I we estimated the column density ( $N$ ) and the excitation temperature ( $T_{\text{ex}}$ ) of the water molecules in two early M type stars, AK Cap and V Hor. The water spectra of these stars were fitted by synthesized spectra using a plane-parallel model. We apply the same method for SAO 163310 (M3); the results are indicated in table 6. The column densities of these stars are as uncertain as one order of the magnitude due to the low spectral resolution of the IRTS/NIRS ( $\lambda/\Delta\lambda \sim 15$ ). These three early M type stars show relatively strong  $\text{H}_2\text{O}$  absorption bands among the stars with similar spectral types (Paper I). Therefore, the resultant column densities are rather high compared to the other stars of similar types. Hinkle and Barnes (1979) and Yamamura et al. (1999b) interpreted the observations of the water bands in the Mira variables in terms of two molecular layers. We list the parameters of both layers in table 6. Hinkle and Barnes (1979) analyzed the high-resolution spectra ( $\lambda/\Delta\lambda =$  a few tens of thousands) of the Mira variable, R Leo, at  $K$  and  $H$  bands, and found two radial-velocity components of water lines. One component has an excitation temperature of 1750 K; the other component is about 1150 K. Yamamura et al. (1999b) fitted the water bands taken by the ISO/SWS (Short-Wavelength Spectrometer) in  $\alpha$  Cet and Z Cas using the “slab” model consisting of two water-vapor layers. They stated that the layer with  $T_{\text{ex}} = 2000$  K should be as large as  $2 R_*$  in order to reproduce the emission band seen at  $3.5\text{--}4.0 \mu\text{m}$  in  $\alpha$  Cet. The cool layer is responsible for the absorption

Table 6. The observations of near-infrared water spectra and SiO masers.

Name	Type	$N(\text{H}_2\text{O}) \text{ cm}^{-2}$	$T_{\text{ex}}(\text{H}_2\text{O}) \text{ K}$	SiO masers			$d(\text{pc})$	References
				$J=1-0$ $v=1$	$J=1-0$ $v=2$	$J=2-1$ $v=1$		
AK Cap	..... Lb	$5 \times 10^{19}$	1000–1500	N	N	N	497	Paper I, this work
SAO 163310	..... .	$1 \times 10^{20}$	1000–1500	N	N	N		Paper I, this work
V Hor	..... SRb	$1 \times 10^{20}$	1000–1500	N			336	Paper I, (4)
$\beta$ Peg	..... Lb	$7 \times 10^{18}$	1250	N	N		61	(1), (5)
g Her	..... SRb	$2 \times 10^{19}$	1250	N	N		111	(1), (5)
SW Vir	..... SRb	$3 \times 10^{19}$	1250	N	N	D	143	(1), (5), (6)
R Leo	warm Mira	$< 5 \times 10^{19} - 3 \times 10^{20}$	1700	D		D	101	(2), (7), (8)
	cool	$2 \times 10^{21} - 2 \times 10^{22}$	1150–1200					
$o$ Cet	hot Mira	$3 \times 10^{21}$	2000	D		D	128	(3), (8), (9)
	cool	$3 \times 10^{20}$	1400					
Z Cas	hot Mira	$3 \times 10^{21}$	2000					(3), (10)
	cool	$1 \times 10^{21}$	1200					

Note. “ $d$ ” indicates the distance to the star based on the Hipparcos and Tycho catalogues (1997). Hinkle and Barnes (1979) and Yamamura et al. (1999b) measured water spectra with two components of water layers, and both layers are indicated individually. The phase dependence of density and temperature is detected in R Leo. In the column in SiO maser, D is detection and N is non-detection. References (1)–(3) are for the water observations and references (4)–(10) are for the SiO maser observations; numbers in parentheses correspond as follows:

- (1) Tsuji et al. (1997),
- (2) Hinkle and Barnes (1979),
- (3) Yamamura et al. (1999b),
- (4) Allen et al. (1989),
- (5) Alcolea et al. (1990),
- (6) Herpin et al. (1998),
- (7) Heske (1989),
- (8) Nyman and Olofsson (1986),
- (9) Buhl et al. (1974),
- (10) Spencer et al. (1981).

feature between 2.5 and 3.5  $\mu\text{m}$ . In the case of Z Cas, the hot layer is located around  $1 R_*$  and both hot and cool layers contribute to the absorption. Hinkle and Barnes (1979) mention that the 1750 K layer is located near the photosphere. This layer may be identical to the 2000 K layer at  $1-2 R_*$  in Yamamura et al. (1999b). The cool layer with  $T_{\text{ex}} = 1200-1400 \text{ K}$  of Miras in Yamamura et al. (1999b) is as large as  $2 R_*$  or larger. Tsuji et al. (1997) also showed that the layer with an excitation temperature of about 1000 K is located at  $\sim 2 R_*$  in irregular and semi-regular variables. We note that according to the “slab” model, when the water layer with  $T_{\text{ex}} = 1500 \text{ K}$  is extended to  $3 R_*$ , or the layer with  $T_{\text{ex}} = 1000 \text{ K}$  to  $5 R_*$ , the water spectra should be observed in emission around 2.7  $\mu\text{m}$ , which is not the case for the present sample. We suppose that the layers with temperatures between 1000 and 1500 K in the stars in table 6 lie around  $2 R_*$ .

Table 6 shows that the stars with the SiO maser have a water column density higher than  $3 \times 10^{19} - 3 \times 10^{20} \text{ cm}^{-2}$ , and non-detected stars have a column density lower than

$5 \times 10^{19} \text{ cm}^{-2}$ . The column densities listed in table 6 vary by more than one order of magnitude among the stars. It is difficult to extend the water layer with the excitation temperature above 1000 K in such a large scale, as discussed above. Thus, the large difference in the water column density should be attributed to the difference in the water density in the stars. The density of the hydrogen molecules in the outer atmosphere can be estimated by dividing the water column densities by the  $\text{H}_2\text{O}$  abundance and the thickness of the layer. An analysis based on the spherical model should be required to make a more accurate estimate, but in this paper we use the numbers derived from a slab model for a rough estimate. The density is probably inhomogeneous in the outer atmosphere, and the SiO maser might be excited in clumps with high-density in the outer atmosphere, as suggested by Langer and Watson (1984). Thus, we try to estimate a lower limit of the density. The  $\text{H}_2\text{O}$  abundance ratio calculated with thermal equilibrium is in the order of  $10^{-4}$  (Tsuji 1964). As a representative value, we

adopt a relatively large  $\text{H}_2\text{O}$  abundance of Barlow et al. (1996),  $\text{H}_2\text{O}/\text{H}_2 = 8 \times 10^{-4}$ . We assume that the size of the  $\text{H}_2\text{O}$  layer is  $1 R_*$  in line of sight, based on the estimated location of the water layer of 1000–1500 K at  $\sim 2 R_*$ . The stellar radius,  $R_*$ , is between  $3 \times 10^{13}$  and  $5 \times 10^{13}$  cm in Mira variables (Diamond et al. 1994), and is estimated as  $3 \times 10^{13}$  cm for a semi-regular variable using Tuthill, Haniff, and Baldwin (1999) and Hipparcos and Tycho Catalogues (1997). We adopt  $5 \times 10^{13}$  cm for the stellar radius for all stars. With these values we obtain  $10^9$ – $10^{10}$   $\text{cm}^{-3}$  for a lower limit of the molecular hydrogen density, corresponding to a water column density of  $3 \times 10^{19}$ – $3 \times 10^{20}$   $\text{cm}^{-2}$ .

The estimated number of  $n(\text{H}_2) = 10^9$ – $10^{10}$   $\text{cm}^{-3}$  is roughly in agreement with the hydrogen density where recent theoretical studies predict that the maser intensity increases drastically (Bujarrabal 1994a; Doel et al. 1995). Bujarrabal (1994a) showed that the SiO maser intensity increases by four orders of magnitudes at the hydrogen densities of  $n(\text{H}_2) \sim 10^8$ – $10^9$   $\text{cm}^{-3}$ . Doel et al. (1995) also showed that the maser gain coefficient (gain per unit amplification path length) increases steeply at  $n(\text{H}_2) \sim 5 \times 10^9$   $\text{cm}^{-3}$ . Therefore, the probability of the SiO maser detection may be prescribed by the critical density of about  $10^9$ – $10^{10}$   $\text{cm}^{-3}$ . However, the critical density at the “spots” where the SiO maser is excited may be even higher if the maser is excited in high-density clumps (Langer, Watson 1984).

Figure 4 shows the correlation between  $C_{12/2.2}$  and the SiO maser intensity, which implies the relation between the density and the excitation of the SiO masers.  $C_{12/2.2}$  is a measure of the dust mass-loss rate in the innermost region of the circumstellar envelope. The mass-loss rate in this region is expected to increase with the density in the outer atmosphere. Therefore, the correlation between  $C_{12/2.2}$  and SiO maser intensity also implies that the maser excitation is related to the density in the outer atmosphere.

Apart from the density, there might be other possibilities which affect the amplification of the SiO masers and lead to the dependence of detection rate on the variable types. For example, Hinkle, Lebzelter, and Scharlach (1997) show that the amplitude of the velocity variation depends on the amplitude of visual magnitudes. The velocity structure might vary depending on the strength of pulsation, which could result in the coherent path length for maser amplification. Further observational studies in the infrared region with high-resolution spectroscopic observations are required to investigate the effects of the velocity structure on the maser excitation.

## 7. Summary

The IRTS provided a large number of stellar spectra without interference from the terrestrial atmosphere.

These data enable us a systematic study of the relation between the SiO maser excitation and the conditions of the outer atmosphere. The IRTS measured the water index,  $I_{\text{H}_2\text{O}}$ , in red giants, which is an indicator of the water column density in the outer atmosphere. In 59 stars selected from the objects observed by the IRTS, the SiO maser lines were detected in 27 stars. Stars with deep water absorption ( $I_{\text{H}_2\text{O}}$  larger than  $\sim 0.1$ ) mostly show the SiO maser lines, and are mostly Mira variables among those with known spectral type. The SiO maser intensity is found to increase with the color,  $C_{12/2.2}$  and  $I_{\text{H}_2\text{O}}$ .

Stars with  $I_{\text{H}_2\text{O}}$  larger than  $\sim 0.1$  mostly show SiO masers, and the stars with SiO maser activity have a water column density higher than  $3 \times 10^{19}$ – $3 \times 10^{20}$   $\text{cm}^{-2}$ , while non-detected stars show values smaller than  $5 \times 10^{19}$   $\text{cm}^{-2}$ . A lower limit of the molecular hydrogen density corresponding to the water column density is estimated to be  $10^9$ – $10^{10}$   $\text{cm}^{-3}$ . This number is roughly comparable to the critical gas density predicted by models where the SiO masers are excited (Bujarrabal 1994a; Doel et al. 1995). If the SiO masers are excited in high-density clumps (Langer, Watson 1984), the critical density would be even higher than the values which we derived here.

The color  $C_{12/2.2}$  well-correlates with the SiO maser intensities.  $C_{12/2.2}$  is probably influenced by the density of the outer atmosphere. The relation  $C_{12/2.2}$  with the SiO masers also suggests that the density of the outer atmosphere is one of the key parameters in SiO maser excitation.

We would like to thank the staff of Nobeyama Radio Observatory for their support. We also appreciate Drs. S. Deguchi, O. Kameya, H. Izumiura, and T. Fujii for their suggestions for the observations. M.M. thanks the Research Fellowships of the Japan Society for the Promotion of Science for the Young Scientists. I.Y. acknowledges the financial support from a NWO PIONIER grant.

## References

- Alcolea J., Bujarrabal V., Gómez-González J. 1990, A&A 231, 431
- Alcolea J., Pardo J.R., Bujarrabal V., Bachiller R., Barcia A., Colomer F., Gallego J.D., Gómez-González J. et al. 1999 A&AS 139, 461
- Allen D.A., Hall P.J., Norris R.P., Troup E.R., Wark R.M., Wright A.E. 1989, MNRAS 236, 363
- Barlow M.J., Nguyen-Q-Rieu, Truong-Bach, Cernicharo J., González-Alfonso E., Liu X.-W., Cox P., Sylvester R.J. et al. 1996, A&A 315, L241
- Buhl D., Snyder L.E., Lovas F.J., Johnson D.R. 1974, ApJ 192, L97
- Bujarrabal V. 1994a, A&A 285, 953
- Bujarrabal V. 1994b, A&A 285, 971

- Cohen M. 1997 Diffuse Infrared Radiation and the IRTS, ed H. Okuda, T. Matsumoto, T.L. Roellig, ASP Conf. Ser., 124, p61
- Deguchi S., Iguchi T. 1976, PASJ 28, 307
- Diamond P.J., Kembell A.J., Junor W., Zensus A., Benson J., Dhawan V. 1994, ApJ 430, L61
- Doel R.C., Gray M.D., Humphreys E.M.L., Braithwaite M.F., Field D. 1995, A&A 302, 797
- Elitzur M. 1980, ApJ 240, 553
- ESA 1997, The Hipparcos and Tycho Catalogue
- Habing H.J. 1996, A&AR 7, 97
- Haikala L.K. 1990 A&AS 85, 875
- Herpin F., Baudry A., Alcolea J., Cernicharo J. 1998, A&A 334, 1037
- Heske A. 1989, A&A 208, 77
- Hinkle K.H., Barnes T.G. 1979, ApJ 227, 923
- Hinkle K.H., Lebzelter T., Scharlach W.W.G. 1997 AJ 114, 2686
- Hyland A.R., 1974, in Highlights of Astronomy, vol. 3 (IAU) p307
- Izumiura H., Deguchi S., Hashimoto O., Nakada Y., Onaka T., Ono T. Ukita N., Yamamura I. 1994, ApJ 437, 419
- Joint IRAS Working Group 1988, IRAS Point Source Catalog (USGPO, Washington DC) (IRAS-PSC)
- Justtanont K., Feuchtgruber H., de Jong T., Cami J., Waters L.B.F.M., Yamamura I., Onaka T. 1998, A&A 330, L17
- Kholopov P.N., Samus N.N., Frolov M.S., Goranskij V.P., Gorynya N.A., Kireeva N.N., Kukarkina N.P., Kurochkin N.E. et al. 1988, General Catalogue of Variable Stars, 4th ed (Nauka Publishing House, Moscow) (GCVS)
- Kwan J., Scoville N. 1974, ApJ 194, L97
- Langer S.H., Watson W.D. 1984, ApJ 284, 751
- Le Sidaner P., Le Bertre T. 1993, A&A 278, 167
- Le Sidaner P., Le Bertre T. 1996, A&A 314, 896
- Matsuura M., Yamamura I., Murakami H., Freund M.M., Tanaka M. 1999, A&A 348, 579 (Paper I)
- Miyoshi M., Matsumoto K., Kameno S., Takaba H., Iwata T. 1994, Nature 371, 395
- Murakami H., Freund M.M., Ganga K., Guo H.F., Hirao T., Hiromoto N., Kawada M., Lange A.E. et al. 1996, PASJ 48, L41
- Noda M., Matsumoto T., Murakami H., Kawada M., Tanaka M., Matsuura S., Guo H.F. 1996, Proc. SPIE 2817, 248
- Nyman L.-Å., Olofsson H. 1986, A&A 158, 67
- Roellig T., Mochizuki K., Onaka T., Tanabe T., Yamamura I., Yuen L.M. 1996, Proc. SPIE 2817, 258
- Ryde N., Eriksson K., Gustafsson B. 1999, A&A 341, 579
- Smithsonian Astrophysical Observatory Star catalog 1966, (Smithsonian Institution, Washington DC) (SAO)
- Spencer J.H., Winnberg A., Olton F.M., Schwartz P.R., Matthews H.E., Downes D. 1981 AJ, 86, 329
- Stephenson C.B. 1984, General Catalog of S Stars, 2ed, Publication of Warner & Swasey Observatory
- Stephenson C.B. 1989, General Catalog of Cool Galactic Carbon Stars, 2ed, Publication of Warner & Swasey Observatory
- Tsuji T. 1964, Ann. Tokyo Astr. Obs. 9, 1
- Tsuji T., Ohnaka K., Aoki W., Yamamura I. 1997, A&A 320, L1
- Tuthill P.G., Haniff C.A., Baldwin J.E. 1999, MNRAS 306, 353
- van der Veen W.E.C.J., Habing H.J. 1988, A&A 194, 125
- Whitelock P., Menzies J., Feast M., Marang F., Carter B., Roberts G., Catchpole R., Chapman J. 1994, MNRAS 267, 711
- Woitke P., Helling Ch., Winters J.M., Jeong K.S. 1999, A&A 348, L17
- Yamamura I., the IRTS Team 1997, in Diffuse Infrared Radiation and the IRTS, ed H. Okuda, T. Matsumoto, T.L. Roellig, ASP Conf. Ser. 124, p72
- Yamamura I., de Jong T., Onaka T., Cami J., Waters L.B.F.M. 1999a, A&A 341, L9
- Yamamura I., de Jong T., Cami J. 1999b, A&A 348, L55
- Yamamura I., de Jong T. 2000, ESA SP-456 in press